Cerebral Cortex October 2015;25:3420–3433
doi:10.1093/cercor/bhu157
Advance Access publication July 17, 2014

Characterization of Panglial Gap Junction Networks in the Thalamus, Neocortex, and Hippocampus Reveals a Unique Population of Glial Cells

Stephanie Griemsmann[1,†], Simon P. Höft[1,†], Peter Bedner[1], Jiong Zhang[1], Elena von Staden[1], Anna Beinhauer[1], Joachim Degen[2], Pavel Dublin[1], David W. Cope[3], Nadine Richter[4], Vincenzo Crunelli[3], Ronald Jabs[1], Klaus Willecke[2], Martin Theis[1], Gerald Seifert[1], Helmut Kettenmann[4] and Christian Steinhäuser[1]

[1]Institute of Cellular Neurosciences, Medical Faculty, University of Bonn, 53105 Bonn, Germany, [2]Life and Medical Sciences (LIMES) Institute, Molecular Genetics, University of Bonn, 53115 Bonn, Germany, [3]School of Biosciences, Cardiff University, Cardiff CF10 3AX, UK and [4]Max-Delbrück-Center for Molecular Medicine, Cellular Neuroscience, 13092 Berlin, Germany

Address correspondence to Christian Steinhäuser, PhD, University of Bonn, Institute of Cellular Neurosciences, Sigmund Freud Strasse 25, D-53105 Bonn, Germany. Email: christian.steinhaeuser@ukb.uni-bonn.de

[†]These authors contributed equally to this work.

The thalamus plays important roles as a relay station for sensory information in the central nervous system (CNS). Although thalamic glial cells participate in this activity, little is known about their properties. In this study, we characterized the formation of coupled networks between astrocytes and oligodendrocytes in the murine ventrobasal thalamus and compared these properties with those in the hippocampus and cortex. Biocytin filling of individual astrocytes or oligodendrocytes revealed large panglial networks in all 3 gray matter regions. Combined analyses of mice with cell type-specific deletion of connexins (Cxs), semiquantitative reverse transcription-polymerase chain reaction (RT-PCR) and western blotting showed that Cx30 is the dominant astrocytic Cx in the thalamus. Many thalamic astrocytes even lack expression of Cx43, while in the hippocampus astrocytic coupling is dominated by Cx43. Deletion of Cx30 and Cx47 led to complete loss of panglial coupling, which was restored when one allele of either Cxs was present. Immunohistochemistry revealed a unique antigen profile of thalamic glia and identified an intermediate cell type expressing both Olig2 and Cx43. Our findings further the emerging concept of glial heterogeneity across brain regions.

Keywords: astrocytes, connexin, genetic deletion, heterogeneity, oligodendrocytes

Introduction

Gap junction channels are composed of connexin (Cx) proteins, which are differentially expressed between cell types, during development and across brain regions (Dermietzel et al. 1989; Kunzelmann et al. 1999; Nagy and Rash 2000; Schools et al. 2006; Giaume et al. 2010). Astrocytes express Cx43 (gene name, *Gja1*), Cx30 (*Gjb6*) and Cx26 (*Gjb2*), while oligodendrocytic gap junction channels are formed by Cx47 (encoded by the gene *Gjc2*) and Cx32 (encoded by *Gjb1*). In addition to interastrocytic (A:A) and interoligodendrocytic (O:O) coupling, recent evidence suggests that astrocytes and oligodendrocytes in vivo also form functional gap junction networks (GJNs) (A:O; panglial coupling), both in white and gray matter (Maglione et al. 2010; Wasseff and Scherer 2011; Tress et al. 2012). Gap junctional communication between oligodendrocytes seems to be crucial for proper myelination and axonal survival (Nualart-Marti et al. 2013). Astrocytic GJNs fulfill a variety of important functions, including regulation of the K^+ and glutamate homeostasis and delivery of energy metabolites to sustain synaptic transmission (Wallraff et al. 2006; Rouach et al. 2008; Pannasch et al. 2011, reviewed by Theis and Giaume 2012; Pannasch and Rouach 2013). The molecular and functional data available as well as antibody staining (Nagy et al. 1997) led to the concept that Cx43 is abundantly expressed and present in all astrocytes throughout the brain.

However, so far the functional expression of Cxs has only been analyzed in a few brain regions, for example, the hippocampus, neocortex, cerebellum, and corpus callosum. Despite the eminent function of the thalamus in processing sensory information and its involvement in sleep-related rhythms (Steriade 2006; Crunelli and Hughes 2010), little is known about the functional properties of glial cells in this area. In the ventrobasal thalamic nuclei, which receive sensory input from the vibrissae and project to the barrel cortex (Bourassa et al. 1995; Bokor et al. 2008), astrocytic Ca^{2+} oscillations were reported to drive neuronal excitation. Moreover, long-term enhancement of astrocytic glutamate release was shown to be dependent on the activation of metabotropic glutamate receptor and Ca^{2+} elevation in astrocytes (Parri et al. 2001; Pirttimaki et al. 2011, 2013). Here we set out to characterize glial gap junction coupling in these nuclei, combining tracer filling in mice with cell type-specific deletion of Cxs, semiquantitative reverse transcription-polymerase chain reaction (sqRT-PCR) and western blotting. In addition, immunohistochemistry was applied to investigate the antigen profile of thalamic astrocytes. Our findings demonstrate that thalamic astrocytes display properties, which significantly differ from those seen in other brain regions and identify an intermediate cell type coexpressing astroglial and oligodendroglial proteins. This insight supports the emerging view that astrocytes in vivo comprise a heterogeneous cell population (Matyash and Kettenmann 2010; Zhang and Barres 2010) whose physiological significance still has to be defined.

Materials and Methods

Animals

Experiments were performed in C57Bl6J (Charles River, Wilmington, USA), Cx43kiECFP (Degen et al. 2012), Cx30kiLacZ (Teubner et al. 2003), Cx30kiLacZ; Cx47kiEGFP (Tress et al. 2012), human glial fibrillary acidic protein-enhanced green fluorescent protein (hGFAP-EGFP) (Nolte et al. 2001), PLP-GFP (Fuss et al. 2000), Cx30kiLacZ; Cx43fl/fl; hGFAP-Cre (Wallraff et al. 2006) and Cx26fl/fl; nestin-Cre mice (Nagy et al. 2011). Animals of either sex were investigated at postnatal day (p) 30–60 if not indicated otherwise. Mice were kept under standard housing conditions. All experiments were carried out in accordance with local, state, and European regulations.

Slice Preparation

Animals were anesthetized with Isoflurane (Abbott, Wiesbaden, Germany), killed by decapitation and the brains were quickly removed. The brains were placed in ice cold preparation solution containing (in mM): 87 NaCl, 2.5 KCl, 1.25 NaH_2PO_4, 25 $NaHCO_3$, 7 $MgCl_2$, 0.5 $CaCl_2$, 25 glucose, 75 sucrose and bubbled with carbogen (95% O_2/5% CO_2). If not stated otherwise chemicals were purchased from Sigma-Aldrich (Taufkirchen, Germany). Using a vibratome (VT1200S, Leica, Nussloch, Germany; HM650V, Microm International, Walldorf, Germany), horizontal and coronal slices containing the ventroposteromedial (VPM) and ventroposterolateral (VPL) nuclei of the thalamus, the hippocampus and cortex were obtained. Slice thickness was 200 µm. Slices were stored at 35°C for 20 min, cooled down to room temperature and transferred into artificial cerebrospinal fluid (ACSF) containing (in mM): 126 NaCl, 3 KCl, 2 $MgSO_4$, 2 $CaCl_2$, 10 glucose 1.25 NaH_2PO_4 and 26 $NaHCO_3$ (room temperature). For some experiments slices were incubated in ACSF supplemented with 1 µM sulforhodamine 101 (SR101; Molecular Probes, Life Technologies, Darmstadt, Germany) at 35°C for 20 min.

Electrophysiological Recordings

For recordings and tracer coupling experiments, slices were transferred to a recording chamber and continuously perfused with carbogenized ACSF. Cells were visualized using an upright microscope equipped with infrared DIC (Eclipse E600FN or Eclipse FN1, Nikon, Düsseldorf, Germany; Axioskop2, Zeiss, Jena, Germany) at 60-fold magnification. Whole-cell voltage clamp experiments were performed on cells identified by endogenous fluorescence or staining with the astrocyte marker SR101 (Nimmerjahn et al. 2004; Kafitz et al. 2008). Pipettes were fabricated from borosilicate glass (Science Products) and had a resistance of 2–6 MΩ when filled with internal solution containing (in mM): 130 K-gluconate, 1 $MgCl_2$, 3 Na_2-ATP, 20 HEPES, 10 ethyleneglycol-bis (2-aminoethylether)-*N*,*N*,*N*′,*N*′-tetra acetic acid, pH 7.2 supplemented with the tracer 0.5% *N*-biotinyl-L-lysine (Biocytin, Sigma-Aldrich). Currents were recorded employing either an EPC-7, EPC-8, or EPC-10 patch-clamp amplifier (Heka, Lambrecht, Germany) and monitored by TIDA software (Heka). Data were sampled at 6–30 kHz and filtered at 3–10 kHz. Input and series resistance were regularly checked by applying +10 mV pulses. The holding potential was –80 mV. Tracer filling was performed for 20 min, afterwards slices were fixed in 4% paraformaldehyde (PFA) in 0.1 M phosphate buffered saline (PBS), pH 7.4 at 4°C.

Immunohistochemistry

Mice were anesthetized by intraperitoneal injection of 80 mg/kg Ketamine hydrochloride (Medistar, Ascheberg, Germany) and 1.2 mg/kg Medetomidine hydrochloride (CP Pharma, Burgdorf, Germany) and transcardially perfused with PBS followed by 4% PFA. Brains were removed, postfixed and cut on a vibratome (VT1200S, Leica) into horizontal slices (40 µm) and stored in PBS at 4°C for subsequent staining. Slices were blocked for 2–4 h at room temperature in PBS containing 2% Triton X-100 and 10% normal goat serum (NGS; Millipore). The first antibodies were incubated in PBS containing 0.1% Triton X-100 and 2% NGS at 4°C overnight; rabbit-α-β-Gal (Molecular Probes, A11132) 1:400; mouse-α-GFP (Invitrogen, Life Technologies, Darmstadt, Germany, A11120) 1:500; rabbit-α-Olig2 (Millipore, Darmstadt, Germany; AB9610) 1:1000; mouse-α-GS (Millipore, MAB302) 1:200; rabbit-α-Iba1 (Wako, Neuss, Germany; 019-19741) 1:400; mouse-α-NeuN (Millipore, MAB377) 1:200; rabbit-α-NG2 (Millipore, AB 5320) 1:100; goat-α-GFP [fluorescein isothiocyanate (FITC)] (Abcam, Cambridge, UK; ab6662-100) 1:500; chicken-α-GFP 1:600 (Abcam; ab13970). The next day slices were washed 3 times in PBS and incubated with the corresponding secondary antibodies in the antibody solution for 1.5 h at room temperature; goat-α-mouseA647 1:500; goat-α-rabbitA647 1:500; donkey-α-rabbitA647 1:500; goat-α-rabbitAlexa594 1:500-1:800; goat-α-mouseAlexa488 1:600, goat-α-chickenAlexa488 1:500 (all antibodies from Invitrogen). Slices were washed 3 times and incubated with Hoechst (Molecular Probes) (1:100 in dH_2O) or Draq5 (Biostatus, Shepshed, UK) (1:1000 in PBS) for nuclei staining, washed again and mounted on coverslides with Aquapolymount (Polysciences Europe, Eppelheim, Germany).

Biocytin was visualized with Streptavidin-Cy3 (Sigma) 1:300, -Cy2 1:100 or -Cy5 (Jackson ImmunoResearch, Suffolk, UK) 1:200 applied in the staining protocol above. Additionally, for the immunohistochemical analysis of the biocytin injected cells 2–5% BSA was added to the blocking and antibody solutions, secondary antibodies were incubated for 2 h at room temperature. Images were acquired at a 1–2 µm interval using a fluorescence microscope (Axiophot, Zeiss, Jena, Germany) employing MetaVue software, a confocal Leica TCS NT or a confocal Leica SPE microscope.

Evaluation of Reporter Expression in Acute Brain Slices

Brains of adult $Cx43^{ECFP/+}$ and PLP-GFP mice were cut in 200 µm thick slices. Stacks of optical sections were obtained with an SP5 LSM (Leica), equipped with an infrared ultra-short-pulse laser (MaiTai; Spectra Physics, Darmstadt, Germany). Two photon absorption was achieved by excitation of the fluorochromes with femtosecond pulses of infrared light with repetition rates of 80 MHz. The wavelength for dual excitation was adjusted for best signal-to-noise ratio: ECFP/SR101: 870–890 nm (1 W); GFP/SR101: 950 nm (0.5 W). Reflected and transmitted light was collected with 2 channel non-descanned detectors in each light pathway. For GFP/SR101 reflected emission light was separated with an FITC–tetramethylrhodamine isothiocyanate (TRITC) filter cube (Leica). For ECFP/SR101 reflected light was splitted with an yellow fluorescent protein-cyan fluorescent protein filter cube (Leica) and the transmitted emission light was separated by a FITC–TRITC filter combination. Depending on the brain area, volumes of 455 × 455 × 40–200 µm were scanned with a resolution of 1024 × 1024 × 80–400 pixels. Image analysis was performed with Leica LAS AF software.

Semiquantitative reverse transcription-polymerase chain reaction (RT-PCR) for Examination of Hippocampal and Thalamic Cx Levels

C57/BL6J mice were anesthetized and decapitated. Their brains were cut into 200 µm thick slices in horizontal orientation as described above and the whole hippocampi and the ventrobasal thalami were dissected. Total RNA was isolated from the tissue by Trizol (Life Technologies) and dissolved in diethylpyrocarbonate-treated water (10 µL). Genomic DNA was removed by DNase treatment in a mixture containing PCR buffer, 2.5 mM $MgCl_2$, 10 mM dithiothreitol (all Life Technologies), 20 U DNaseI (Roche, Mannheim, Germany) and 40 U RNase inhibitor (Promega, Mannheim, Germany; final volume 20 µL; incubation at 37°C for 30 min). Oligo (dT)25 linked Dynabeads™ (Life Technologies) were used to isolate mRNA. The mRNA was suspended in water (20 µL) and stored at –20°C.

Semiquantitative RT-PCR was performed as a single enzyme procedure using rTth DNA polymerase (TaqMan™ EZ RT-PCR Kit, Applied Biosystems, Darmstadt, Germany). The final reaction volume was 12.5 µL containing 1 µL mRNA, TaqMan™ EZ buffer, 3 × 300 µM dNTPs (2′-deoxyadenosine 5′-triphosphate, 2′-deoxycytidine 5′-triphosphate and 2′-deoxyguanosine 5′-triphosphate), 600 µM 2′-deoxyuridine 5′-

Table 1
Primers for semiquantitative RT-PCR

Gene	Sequence	Position	Product length (bp)	GeneBank accession no.
Gja1(Cx43)	se 5′-TTTGACTTCAGCCTCCAAGGA	–80	79	NM_010288
	as 5′-TCTGGGCACCTCTCTTTCACTTA	–24		
Gja1(Cx43) probe	se 5′-TTCCACCACTTTGGCGTGCCG	–58		
Gjb6(Cx30)	se CGTACACCAGCAGCATTTTCTT	404	78	NM_001010937
	as 5′-ACCCATTGTAGAGGAAGTAGAACACAT	455		
Gjb6 (Cx30) probe	se 5′-CGCATCATCTTCGAAGCCGCCT	427		

Note: "se" and "as" indicate sense and antisense primers. Position 1 is the first nucleotide of the initiation codon. The fluorogenic TaqMan Gjb6 (Cx30)and Gja1(Cx43) probes were labeled at their 5′-end with 6-carboxyfluoresceine (FAM) and at their 3′-end with 6-carboxytetramethylrhodamine (TAMRA).

triphosphate, 3 mM $Mn(OAc)_2$, 1.25 U rTth DNA polymerase, 0.125 U uracil-*N*-glycosylase, 100 nM fluorogenic TaqMan™ probe and 600 nM of *Gja1* and *Gjb6* primers, respectively (Table 1). For β-actin quantification, a Taqman probe/primer mix was used (Applied Biosystems). RT-PCRs for *Gja1*, *Gjb6* and *β-actin* were run in parallel tubes for each sample. Samples were incubated at 50°C (2 min), and first strand synthesis was performed at 60°C (20 min). After denaturation (95°C, 5 min), 40 cycles were performed (denaturation at 94°C, 15 s; primer annealing and extension at 59°C, 60 s). Fluorescence intensity was readout during each annealing/extension step. *Data Analysis*: we determined the expression ratio of *Gja1/β-actin* and *Gjb6/β-actin* genes by comparing threshold cycle (C_T) values of the target gene with those of the reference gene at the same fluorescence emission Rn. The respective amplification efficiencies were determined by the serial dilution method (Seifert et al. 2009).

Western Blot Analysis

Brain tissue of hippocampus and thalamus from C57/BL6J mice were lyzed in modified RIPA lysis buffer (50 mM Tris, 150 mM NaCl, 0.5% Nonidet P40, 0.5% Na-DOC, 1% Triton X-100, pH 7.5) supplemented with protease and phosphatase inhibitor single-use cocktail (Thermo Scientific, St Leon-Rot, Germany; 78443). The tissue samples were homogenized and incubated on ice for 30 min. Samples were centrifuged for 30 min at 13 000*g* at 4°C and the supernatants were transferred into new tubes. Total protein content was assayed with BCA (Pierce, Bonn, Germany) and 30–50 µg of total protein per lane was used. Lysates were mixed with sample buffer (62.5 mM Tris–Cl, pH 6.8, 3% sodium dodecyl sulfate (SDS), 0.01% bromophenol blue, 5% β-mercaptoethanol, 10% glycerol) and heat-incubated for 10 min at 65°C before they were shortly centrifuged at 4°C. Proteins were separated with standard 10–12% SDS-polyacrylamide gel electrophoresis (PAGE) under denaturing conditions and electroblotted onto a PVDF membrane. Membranes were blocked with 5% milk powder in tris-buffered saline (TBS) (pH 7.4) containing 0.05% Tween-20 and incubated overnight at 4°C on a rotator with the following primary antibody solutions: rabbit-anti-Cx43 (1:5000; Sigma), rabbit-anti-Cx30 (Zymed-Invitrogen, Life Technologies) 1:250, mouse-anti-α-tubulin (Sigma) 1:20 000. Secondary antibodies used: goat-anti-mouse HRP conjugate (GE Healthcare, München, Germany) 1:10 000, goat-anti-rabbit HRP conjugate (GE Healthcare) 1:10 000. All antibodies, including secondary antibodies were diluted in 5% milk powder in TBS (pH 7.4) containing 0.05% Tween-20. HRP was visualized with the West Dura substrate (Pierce) and chemiluminescence was detected with the Gene Gnome digital documentation system (Synoptics, Cambridge, UK). Raw data analysis and densitometry were performed with GeneTools quantification software (Synoptics). Cx43 and Cx30 were always measured from the same samples.

Data Analysis

Data are given as mean ±standard error of the mean. Differences between data were tested for significance using Student's *t*-test, Mann–Whitney *U*-test or analysis of variance (ANOVA) followed by Tukey's test, as appropriate. Differences between means were regarded as significant at $P < 0.05$ (*) or $P < 0.01$ (**).

Results

Gap junction coupling is a hallmark of glial cells and plays an important role in brain function, albeit these networks have been characterized only in a few regions yet. Here we employed mouse lines with fluorescently labeled astrocytes and oligodendrocytes to investigate coupling between glial cells in the ventrobasal thalamus (VPL/VPM nuclei) in comparison to neocortex and the stratum radiatum of the hippocampal CA1 region.

Thalamic Glial Cells are Abundantly Coupled

Astrocytes were identified by their passive current pattern, typical morphology and bright EGFP fluorescence in hGFAP-EGFP mice (Fig. 1A_1) (Nolte et al. 2001; Matthias et al. 2003). Biocytin injection into a thalamic astrocyte revealed large networks of cells, which did not further increase beyond the first 2 postnatal weeks (p9–11, 84 ± 13 cells;p13–15, 111 ± 8 cells; p30–60, 108 ± 11 cells; p90–120, 95 ± 8 cells; Fig. 1*C*). The ventrobasal thalamus, particularly the VPL, contains densely packed myelinated fiber tracts. Unexpectedly, in several cases we observed spread of the tracer from the astrocyte into the myelin sheath along the fiber tracts (Fig. 1A_2, *B*, see inset in *B*). Orientation of GJNs along functional entities has been observed previously in the barrel cortex (Houades et al. 2008) and in the olfactory bulb (Roux et al. 2011).

Comparative Analyses of GJNs in the Thalamus, Neocortex, and Hippocampus Reveal Distinct Expression of Cx43 and Cx30

Earlier studies have demonstrated a major impact of Cx43 on the size of GJNs in the hippocampus (Wallraff et al. 2006; Gosejacob et al. 2011). To compare the relevance of Cx43 in thalamic, hippocampal, and cortical astrocytes, tracer coupling was investigated in heterozygous Cx43kiECFP mice, in which one allele of *Gja1* was replaced by ECFP (p30–64; Fig. 2*A*–*C*). In these mice, ECFP is expressed by astrocytes but not by NG2 cells (Degen et al. 2012). In wild-type littermates, biocytin spread to ~80 coupled cells, irrespective of the brain region investigated (Fig. 2D_1). Knockout (ko) of one *Gja1* allele in Cx43kiECFP mice led to a significant decrease in the number of coupled cells in the hippocampus ($Gja1^{+/+}$, 79 ± 9 cells; $Gja1^{ECPF/+}$ 51 ± 10 cells), while in the somatosensory cortex and thalamus no changes in network size were observed (cortex, $Gja1^{+/+}$, 75 ± 9 cells; $Gja1^{ECPF/+}$, 71 ± 9 cells; thalamus, $Gja1^{+/+}$, 79 ± 4 cells; $Gja1^{ECPF/+}$, 87 ± 10 cells) (Fig. 2D_1).

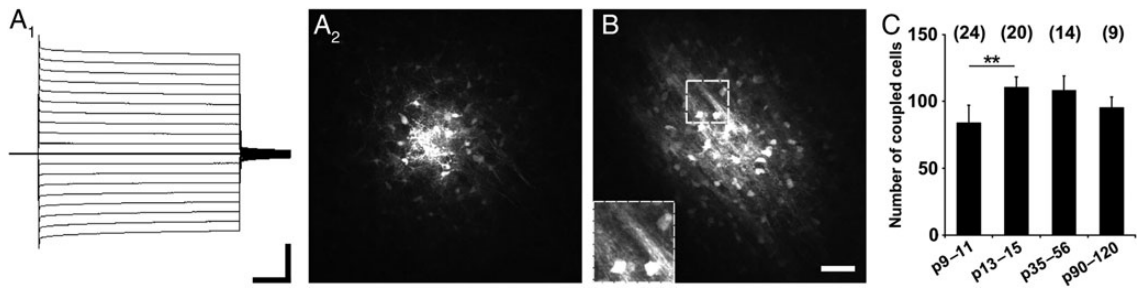

Figure 1. Dye coupling in thalamus. (A_1), Representative current pattern of an EGFP fluorescent astrocyte in hGFAP-EGFP mice. De- and hyperpolarization of the membrane between −160 and +20 mV evoked a passive current pattern in whole-cell voltage clamp mode (10 mV increment, holding potential −80 mV). Scale bar, 10 ms, 5 nA. (A_2) Tracer-coupled glial cells, biocytin spread from the initial cell always revealed large networks. (*B*), The tracer also diffused along presumed myelinated fiber tracts, as shown in the inset. Scale bar, 50 µm. (*C*) Summary of the amount of tracer coupling at different time points. The average GJN size increased between p9–11 and p13–15 and was constant during later development. Number of experiments is given in parentheses. Asterisks indicate statistical significance.

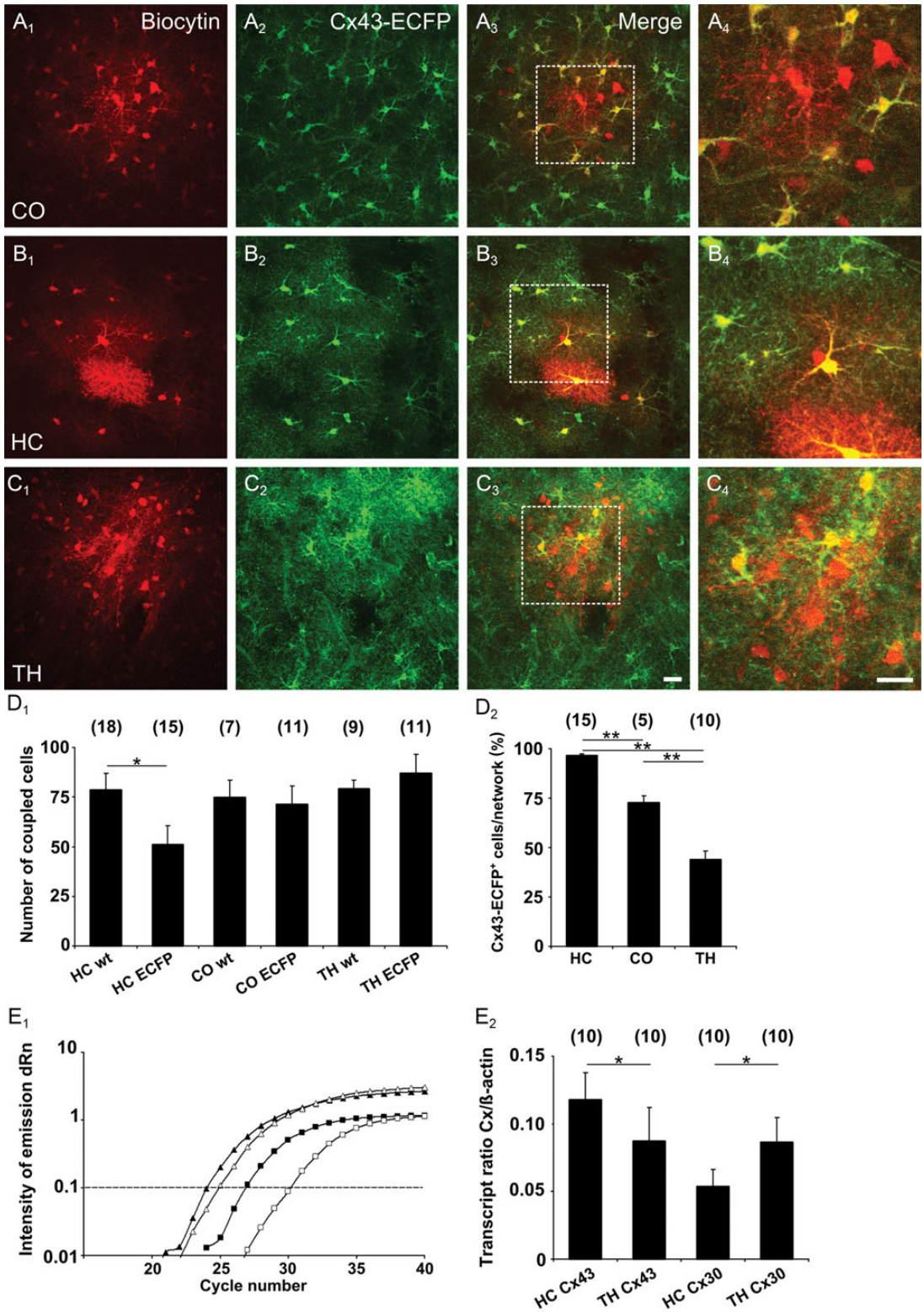

Figure 2. Astrocyte heterogeneity revealed by network analysis in Cx43kiECFP mice. (*A–C*) ECFP$^+$ astrocytes in the cortex (CO), CA1 region of the hippocampus (HC) and thalamus (TH) were filled with biocytin. In heterozygous Cx43 (*Gja1*$^{ECFP/+}$) mice, all brains regions investigated displayed tracer-coupled networks (*A*$_1$, *B*$_1$, *C*$_1$), which contained frequent ECFP$^+$ cells (*A*$_2$, *B*$_2$, *C*$_2$). (*A*$_4$, *B*$_4$, *C*$_4$) Blowups of insets in merged pictures (*A*$_3$, *B*$_3$, *C*$_3$). Colocalization of biocytin and ECFP was observed in many cells in all regions. Scale bars in *C*$_3$ and *C*$_4$ indicate 20 μm. (*D*$_1$) Summary of the extent of biocytin coupling in the corresponding brain regions of wild-type littermates (wt) and heterozygous Cx43 (*Gja1*$^{ECFP/+}$) mice (ECFP). (*D*$_2$), Proportion of tracer-filled cells showing ECFP and biocytin colocalization in the 3 brain regions (HC, 96.6 $\pm$ 0.76%; CO, 72,6 $\pm$ 3.6%; TH, 43.8 $\pm$ 4.6%). Number of investigated GJNs is shown above bars. (*E*$_1$) sqRT-PCR amplification curves of Cx43 (*Gja1*, squares) and β-actin mRNA (triangles) obtained from the hippocampus (filled symbols) and thalamus (open symbols). The difference in threshold cycles between β-actin and Cx43 (ΔRn; taken at the dashed line) for the thalamus was larger than for the hippocampus, consistent with lower Cx43 transcript levels in the former. (*E*$_2$) Transcript ratios Cx43(*Gja1*)/β-*actin* and *Cx30(Gjb6)*/β-*actin* differed significantly between the hippocampus and thalamus. Cx43 expression was higher in the hippocampus while in the thalamus Cx30 predominates. Number of tissue specimens in parentheses. Asterisks indicate statistical significance (*$P < 0.05$, **$P < 0.01$).

Consistently, in these heterozygous Cx43-ECFP mice a vast majority of the biocytin-labeled cells in the hippocampus expressed Cx43, as indicated by expression of the reporter gene ECFP. In contrast, only part of the coupled cells in the thalamus was ECFP$^+$ and the number of ECFP$^+$ cells within cortical GJNs was also lower than in the hippocampus (Fig. 2*D*$_2$). We compared the expression of *Gja1* and *Gjb6* in the thalamus and the hippocampus at the transcript level. As expected, sqRT-PCR revealed a lower *Gja1/β-actin* mRNA ratio in the thalamus (0.09 ± 0.03) versus hippocampus (0.12 ± 0.02). Notably, the *Gjb6/β-actin* mRNA ratio was higher in the thalamus (0.09 ± 0.02) versus hippocampus (0.06 ± 0.01) (Fig. 2*E*). Our data confirm earlier studies showing that Cx43 is predominantly expressed in hippocampal and cortical GJNs. This is in contrast to the thalamus where the majority of coupled cells lack Cx43.

Many Thalamic Astrocytes are Devoid of Cx43

The surprising finding that a majority of coupled cells in the thalamus lacked Cx43-ECFP raised the question of their identity. To address this issue, we assessed the proportion of ECFP$^+$ cells among thalamic astrocytes employing SR101 (Nimmerjahn et al. 2004; Kafitz et al. 2008) and 2-photon laser scanning microscopy in acute slices. Indeed, 50% of the SR101$^+$ cells lacked ECFP (Fig. 3*A*). This clearly differed from the hippocampus where the vast majority of SR101$^+$ cells also expressed ECFP (Fig. 3*B*). To ensure that our data were not distorted through potential SR101 labeling of oligodendrocytes (Wasseff and Scherer 2011), transgenic mice with fluorescence labeling of oligodendrocytes (PLP-GFP mice) (Fuss et al. 2000) were employed. In both brain regions only a few, weakly SR101$^+$ cells were also GFP$^+$ (thalamus, 1.9 ± 0.5%; hippocampus, 1 ± 0.8%) (Fig. 3*C*, *D*). Since these weakly SR101$^+$/GFP$^+$ cells were not visible with

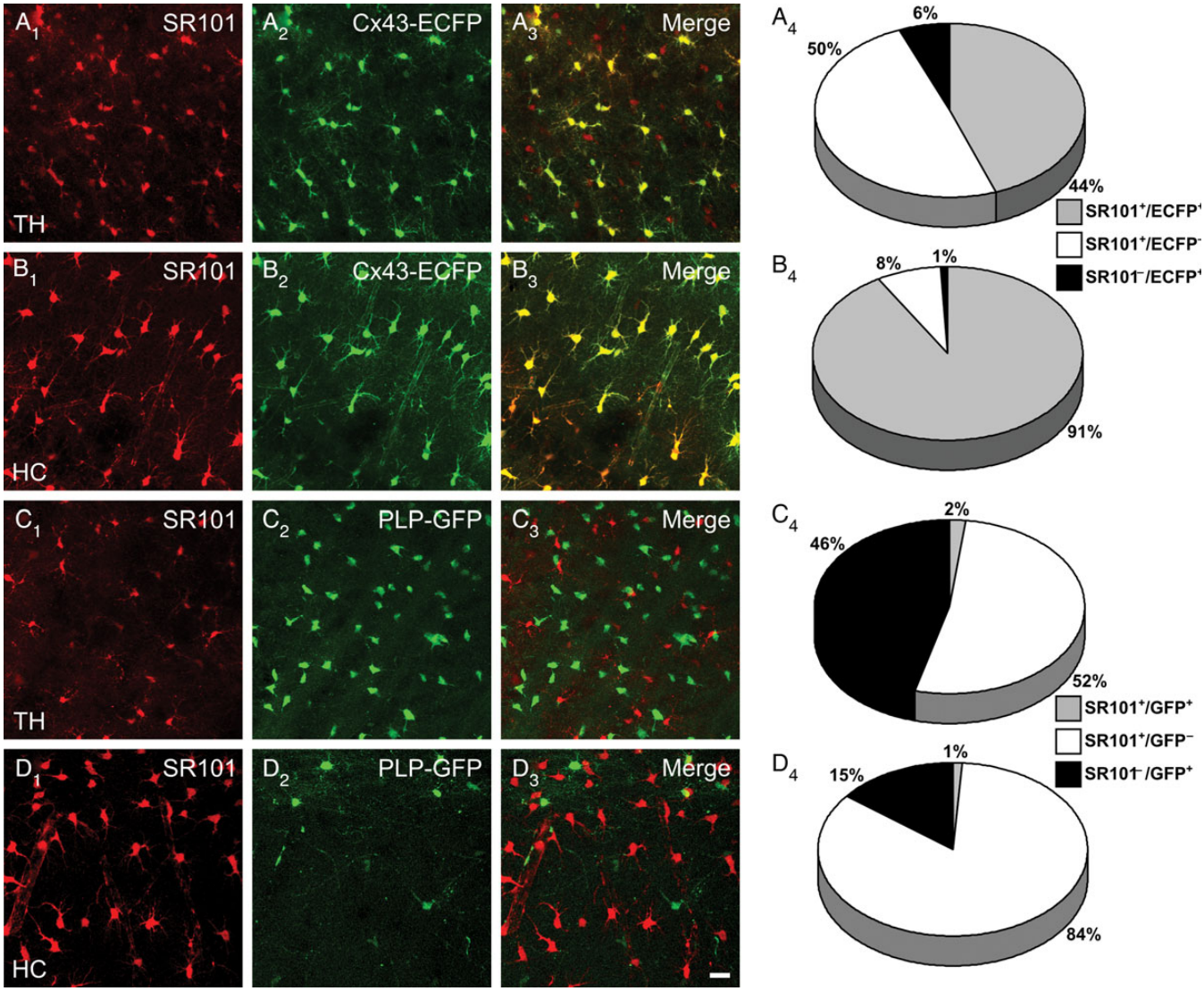

Figure 3. SR101$^+$ astrocytes display differential Cx43-ECFP expression in hippocampus and thalamus. (*A–B*) Two-photon images of SR101 labeled astrocytes in acute brain slices of Cx43$^{ECFP/+}$ mice (*A*$_{1–2}$, *B*$_{1–2}$,). In both regions colocalization of SR101 and ECFP was observed though to a differing extent (*A*$_3$, *B*$_3$). Quantifications of the populations of astrocytes are shown in A$_4$ and B$_4$ (n = 9 and 6 from 3 mice each, respectively). (*C–D*) Astrocyte-specific labeling of SR101 was confirmed in PLP-GFP mice. Acute brain slices of PLP-GFP mice were analyzed in similar experiments as Cx43-ECFP mice (*C*$_{1–2}$, *D*$_{1–2}$), showing only minor overlap of PLP-GFP and SR101 in the thalamus (*C*$_3$, *C*$_4$) or hippocampus (*D*$_3$, *D*$_4$) (n = 11 and 8 from 4 and 3 mice, respectively). Scale bar, 20 μm.

conventional epifluorescence microscopy used at the patch-clamp setups, SR101 was a reliable marker to identify astrocytes. These findings were in line with the assumption that a significant proportion of the thalamic astrocytes lack Cx43.

Thalamic GJNs are Mainly Formed by Cx30

The moderate participation of Cx43-ECFP$^+$ cells in the GJNs and our transcript analysis (Fig. 2) suggested that astrocytic coupling in the thalamus was dominated by Cx30. To investigate the impact of this isoform on thalamic coupling we employed homozygous Cx30kiLacZ mice, in which the coding region of the *Gjb6* gene was replaced by the reporter gene LacZ (Teubner et al. 2003). In these mice biocytin filling of SR101$^+$ thalamic astrocytes showed a drastic decrease in coupling compared with littermate controls (*Gjb6*$^{+/+}$, 81 ± 6 cells; *Gjb6*$^{LacZ/LacZ}$, 22 ± 3 cells) (Fig. 4*A*), and even complete uncoupling in some cases

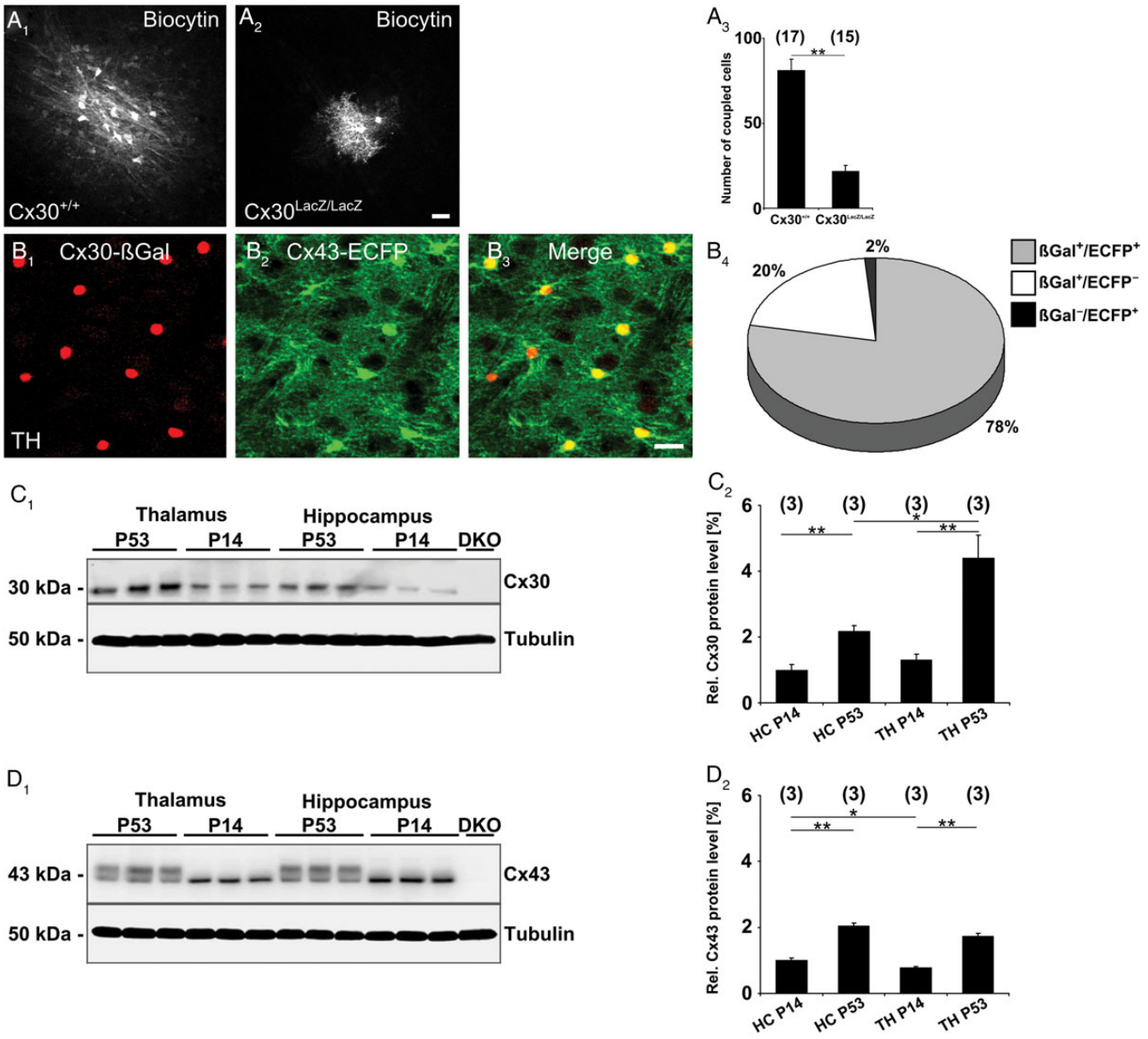

Figure 4. Connexin30 is the predominant gap junction protein in the thalamus. (*A*) Confocal images of biocytin-labeled cells in the thalamus of *Gjb6*$^{+/+}$ mice (*A*$_1$) and *Gjb6*$^{LacZ/LacZ}$ littermates (*A*$_2$). *Gjb6*$^{LacZ/LacZ}$ littermates displayed smaller or no networks, with a bright initially injected cell and only weakly labeled neighboring cells. (*A*$_3$) Networks sizes were decreased by 73% in *Gjb6*$^{LacZ/LacZ}$ versus *Gjb6*$^{+/+}$ mice. Number of experiments is given in parentheses. (*B*) Mice heterozygous for Cx30kiLacZ (*B*$_1$) and for Cx43kiECFP (*B*$_2$) were immunohistochemically analyzed for reporter gene expression in the thalamus. Different populations were observed according to their Cx expression profile. Most cells showed colocalization of the reporters (yellow), but cells expressing only one reporter were also present (red or green) (*B*$_3$, merge). (*B*$_4$) Quantitative summary of Cx reporter expression revealed 3 different astrocytic populations in the thalamus, almost all cells investigated expressed Cx30 (βGal$^+$/ECFP$^+$, 78.1 ± 2.6%; βGal$^+$/ECFP$^-$, 20.4 ± 2.4%; βGal$^-$/ECFP$^+$, 1.5 ± 0.7%, $n = 9$ from 3 mice). Scale bar, 20 μm. (*C*$_1$) Western blot analysis of Cx30 protein levels in the thalamus and hippocampus of C57/Bl6 mice at 2 different time points. Cx30 protein levels increased with age and differ between the 2 brain regions. Antibody specificity was confirmed using the Cx30/Cx43 (*Gjb6*$^{LacZ/LacZ}$;*Gja1*$^{fl/fl}$; *hGFAP-Cre*) double-ko mouse (DKO) as negative control, α-tubulin as a loading control. (*C*$_2$) Normalized protein levels confirmed the increase of Cx30 levels during development, although this was more pronounced in the thalamus. (*D*$_1$) Western blot analysis of Cx43 (C57/Bl6), the 2 bands visible correspond to different phosphorylation status of the protein. (*D*$_2$) Cx43 protein levels were normalized to α-tubulin levels, yielding a lower expression in the thalamus at p14, while in adult animals no difference in Cx43 expression was detected. (*C*$_2$, *D*$_2$; number of mice above bars). Asterisks indicate statistical significance.

($n = 5$; not shown). These findings differed significantly from the hippocampus, where loss of Cx30 decreased coupling only by 22% (Gosejacob et al. 2011). SR101 uptake did not influence tracer coupling in the thalamus (SR101 incubation, 113 ± 8 cells, $n = 12$; control, 106 ± 12 cells, $n = 8$, not shown).

Further experiments performed in mice deficient for Cx30 and Cx 43 (*Gjb6*$^{LacZ/LacZ}$;*Gja1*$^{fl/fl}$;*hGFAP-Cre*) revealed complete disruption of gap junctional communication in 16 out of 18 biocytin-filled thalamic SR101$^+$ cells. Residual coupling (8 ± 6 cells) was observed in 2 cases (not shown). Since Cx26 was reported to be abundantly expressed in the thalamus (Nagy et al. 2011), we examined the potential contribution of Cx26 to GJNs in the thalamus in mice devoid of Cx26 (*Gjb2*$^{fl/fl}$; nestin-Cre). Analysis of biocytin transfer in the hippocampus and thalamus revealed no significant difference between control and Cx26 ko mice (thalamus, control, 150 ± 23 cells, $n = 9$; *Gjb2*$^{fl/fl}$; *nestin-Cre*, 112 ± 17 cells, $n = 11$; hippocampus, control, 91 ± 9 cells, $n = 8$; *Gjb2*$^{fl/fl}$; *nestin-Cre*, 118 ± 14 cells, $n = 9$, not shown). Accordingly, Cx26 does not seem to significantly contribute to functional GJ channels in the brain areas analyzed.

To further investigate Cx expression on a cellular level we performed reporter gene analysis in *Gja1*$^{ECFP/+}$;*Gjb6*$^{LacZ/+}$ mice. Since LacZ is not expressed in the hippocampus of these mice (Gosejacob et al. 2011), experiments were restricted to the thalamus (Fig. 4*B*). Quantification of the overlap of ECFP and β-Gal signal unveiled that almost all (43 051 ± 1627 β-Gal$^+$ cells/mm^3 of 43 719 ± 1457 total cells/mm^3) of the thalamic astrocytes express Cx30, and many of them lack Cx43 (8904 ± 1,117 β-Gal$^+$/ECFP$^-$ cells/mm^3) (Fig. 4B_4). The latter population probably accounts for the uncoupled cells found in the thalamus of Cx30 ko (*Gjb6*$^{LacZ/LacZ}$) mice (cf. above).

Western blot analysis revealed an up-regulation of Cx expression during postnatal development (Fig. 4*C*,*D*). In the hippocampus Cx30 and Cx43 increased 2-fold between p14 and p53, while Cx30 protein levels increased more than 3-fold during this period in the thalamus. Thus, in the adult brain, thalamic Cx30 levels significantly exceed those in the hippocampus, while Cx43 protein content does not differ (Fig. 4C_2,D_2). In conclusion, astrocytic coupling in the adult thalamus is mediated predominantly by Cx30.

Oligodendrocytes and Astrocytes Form Functional Panglial Networks

The experiments so far documented a population of astrocytes in the thalamus lacking Cx43, but abundantly expressing Cx30. Further characterization of cell identity in GJNs was carried out employing hGFAP-EGFP mice. Notably, EGFP was abundantly expressed in both thalamus and hippocampus, although GFAP antibody staining in the thalamus labels only very few cells (not shown; see Frassoni et al. 2000; Parri and Crunelli 2002). Thus, glutamine synthetase (GS) was used as a marker for astrocytes (Norenberg 1979; Sonnewald et al. 1997; Coulter and Eid 2012). GS was expressed by less than half of the biocytin-coupled cells in the thalamus (49 ± 8 of 100 ± 13 cells) while most of the coupled cells in the hippocampal CA1 region were GS$^+$ (106 ± 10 of 129 ± 11 cells) (Fig. 5*A*,*B*). Surprisingly, when staining against Olig2, a transcription factor expressed in cells of the oligodendrocyte lineage (Marshall et al. 2005; Nishiyama et al. 2009; Trotter et al. 2010) we found abundant expression in thalamic and cortical networks (49 ± 8 of 75 ± 7 cells and 62 ± 24 of 102 ± 25 cells, respectively; Fig. 5*C*–*E*). In hippocampal GJNs Olig2 labeling was much less prevalent (19 ± 4 of 129 ± 18 cells) (Fig. 5*C*,*D*). The data indicated participation of oligodendrocytes in GJNs of the 3 brain regions investigated. Furthermore in the hippocampus, GS and Olig2 label distinct cell populations while the overlap in staining as derived from cell counting (Fig. 5*A4*,*C4*) indicated that in the thalamus these markers are not cell type-specific.

In contrast to recent findings in the corpus callosum (Maglione et al. 2010), we never observed NG2$^+$ cells within thalamic, hippocampal, or cortical GJNs (thalamus, 0 of 117 ± 11 cells, $n = 8$; hippocampus, 0 of 136 ± 18 cells, $n = 8$; cortex, 0 of 143 ± 14 cells, $n = 6$). Moreover Iba1$^+$ microglia (thalamus $n = 9$, hippocampus $n = 8$) or NeuN$^+$ neurons (thalamus $n = 9$, hippocampus $n = 6$) never participated in the networks (not shown).

The abundance of Olig2$^+$ cells in thalamic GJNs challenged the concept of pure astrocytic networks. Astrocytic Cxs form heterotopic channels with oligodendrocytic Cxs *in vitro* (Orthmann-Murphy et al. 2007; Magnotti et al. 2011), and recently functional panglial networks have also been observed *in situ* (Maglione et al. 2010; Wasseff and Scherer 2011; Tress et al. 2012). To confirm putative astrocyte–oligodendrocyte coupling, PLP-GFP$^+$ oligodendrocytes or SR101$^+$ astrocytes were patched and tracer spread was quantified. Filling of astrocytes with biocytin in the thalamus und hippocampus revealed abundant coupling (thalamus, 118 ± 15; hippocampus, 133 ± 16; Fig. 6*A*,*C*,E_1). Notably, the GJNs were not significantly smaller when filling oligodendrocytes with the tracer (thalamus, 87 ± 14; hippocampus, 82 ± 15), and coupling did also not differ between brain regions (Fig. 6*B*,*D*,E_1). In a next step we analyzed the proportion of PLP-GFP$^+$ cells in these GJNs and found considerable differences between brain regions. In the thalamus >50% of biocytin-labeled cells were GFP$^+$, while in the hippocampus <14% were GFP$^+$. However, in a given brain region, the proportion of GFP$^+$ cells was the same when injecting an astrocyte or an oligodendrocyte (Fig. 6E_2). Thus, tracer spread into the panglial syncytium was independent of the type of glia initially patched. The diverging contribution of PLP-GFP$^+$ cells to the GJNs in the 2 brain regions obviously reflects the different densities of the PLP-GFP$^+$ cells (Fig. 3*C*,*D*; Fig. 6). Additionally, panglial coupling was investigated prior to the expected onset of Cx30 protein expression (Kunzelmann et al. 1999). Biocytin injection in thalamic astrocytes of p9-11 old PLP-GFP mice revealed abundant panglial coupling (87 ± 18 coupled cells; among them 34% GFP$^+$ cells; $n = 14$; Supplementary Fig. 1). These data directly demonstrate that both in the hippocampus and thalamus, astrocytes and oligodendrocytes form panglial GJNs.

Panglial Coupling in the Thalamus and Hippocampus is Mainly Mediated by Heterotypic Channels Containing Cx30

To investigate the molecular basis of panglial coupling in the thalamus and hippocampus we employed ko mice in which *Gjb6* was replaced by LacZ and *Gjc2* by EGFP (Tress et al. 2012). Cx30 and Cx47 form functional gap junction channels with Cx32 and Cx43, respectively, thus mediating astrocyte to oligodendrocyte coupling (Orthmann-Murphy et al. 2007; Theis and Giaume 2012). Coupling analysis was performed by injecting biocytin in astrocytes from *Gjb6*$^{+/LacZ}$; *Gjc2*$^{EGFP/EGFP}$

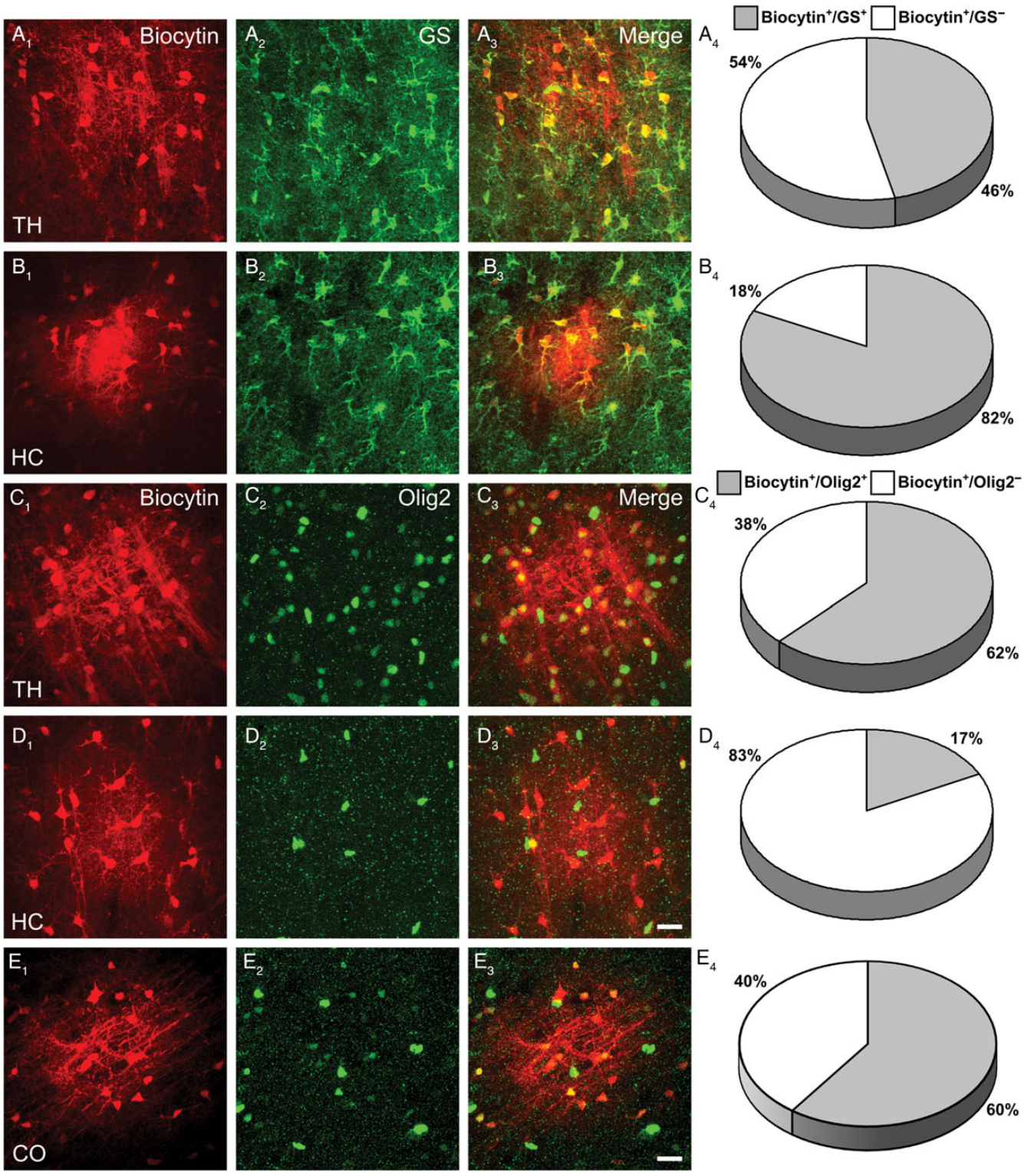

Figure 5. Tracer-coupled GJNs have distinct immunohistochemical properties. Immunostainings of GJNs (A_1-E_1) in hGFAP-EGFP mice in the thalamus, hippocampus and cortex using antibodies against GS (A_2, B_2) and Olig2 (C_2, D_2, E_2). (A_3–E_3) show merged images. Note that networks in the thalamus contained <50% GS^+ cells (A_4, 46.4 ± 5.4%, $n = 10$) but most coupled cells in this region were $Olig2^+$ (C_4, 62.2 ± 8.4%, $n = 10$). In contrast, hippocampal GJNs mainly comprised GS^+ cells (B_4, 81.6 ± 2%, $n = 7$), while only a few cells were $Olig2^+$ (D_4, 17.5 ± 4.6%, $n = 7$). Similar to the thalamus, most of the coupled cells in the neocortex were $Olig2^+$ (E_4, 60 ± 15%, $n = 8$). Scale bar, 20 μm.

(Fig. 7A_1), *Gjb6*$^{LacZ/LacZ}$; *Gjc2*$^{EGFP/EGFP}$ (Fig. 7A_2) and *Gjb6*$^{LacZ/LacZ}$; *Gjc2*$^{+/EGFP}$ mice. In *Gjb6*$^{LacZ/LacZ}$; *Gjc2*$^{EGFP/EGFP}$ mice, many of the biocytin-filled cells lacked coupling (thalamus, 43%; hippocampus, 60%; Fig. 7*B*), with the remaining cells showing only tiny networks (thalamus, 5 ± 1; hippocampus, 5 ± 2 coupled cells; Fig. 7*C*). Deletion of both Gjc2 alleles and one *Gjb6* allele still resulted in large GJNs (thalamus, 166 ± 16; hippocampus, 79 ± 14 coupled cells; Fig. 7*C*), whereas only

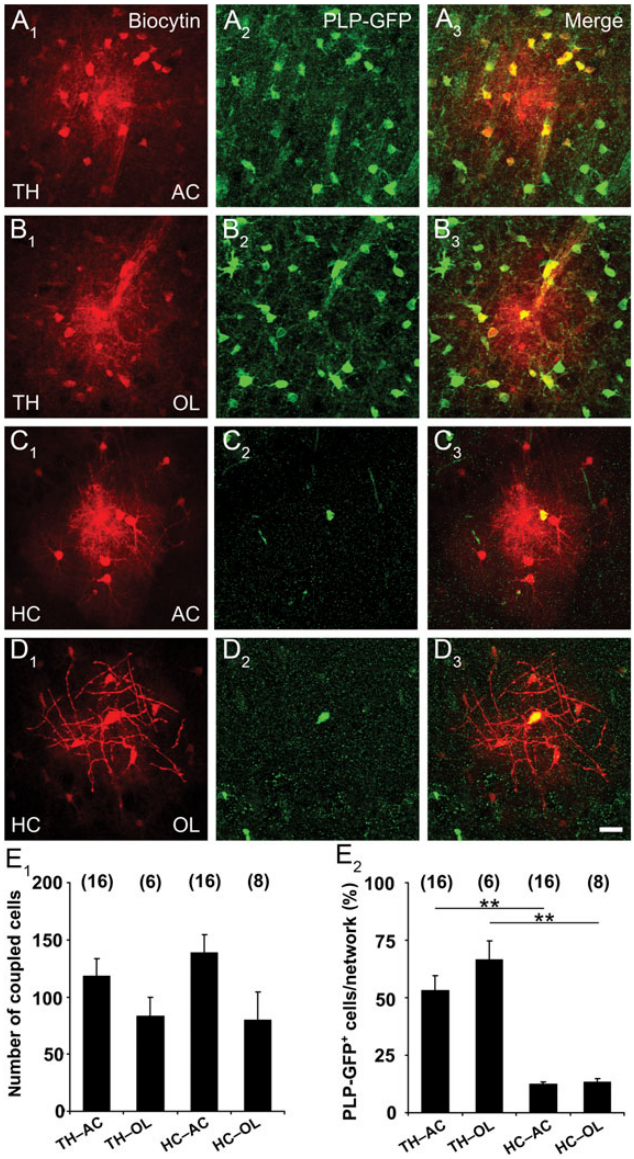

Figure 6. Astrocyte:oligodendrocyte coupling is independent of the initial filled cell-type. (*A–D*) Astrocytes and oligodendrocytes in the thalamus and hippocampus of PLP-GFP mice were identified by SR101 labeling or GFP fluorescence, accordingly. Either astrocytes (*A*, *C*; indicated by AC) or oligodendrocytes (*B*, *D*; as indicated by OL) were tracer-filled (A_1–D_1) and costained for GFP (A_2–D_2) revealing spread of the tracer into PLP-GFP$^+$ oligodendrocytes (A_3–C_3). Notably, all PLP-GFP$^+$ oligodendrocytes injected in the thalamus or hippocampus showed intercellular coupling (B_3, D_3). Scale bar, 20 μm. (E_1) Graph showing the number of coupled cells in the thalamus and hippocampus, depending on whether the injected cell was an astrocyte (AC) or an oligodendrocyte (OL). Size of the GJNs did not differ significantly. (E_2) The proportion of PLP-GFP$^+$ cells in the networks was larger in the thalamus, but independent of the cell type initially filled with the tracer (TH, 53.1 ± 6.4% and 66.5 ± 8.4%, HC: 12.4 ± 1 and 13.4 ± 1.4, injection into AC or OL, respectively). Number of experiments is given above bars. Asterisks indicate statistical significance.

small GJNs were observed in *Gjb6*$^{LacZ/LacZ}$; *Gjc2*$^{+/EGFP}$ mice (thalamus, 28 ± 11; hippocampus, 39 ± 19 coupled cells). The proportion of oligodendrocytes within the GJNs, as assessed by Cx47-EGFP-fluorescence, varied considerably between the different genotypes (Fig. 7*D*). The tiny networks in mice lacking both Cx30 and Cx47 did not contain oligodendrocytes, while panglial networks were observed in thalamus and hippocampus of *Gjb6*$^{+/LacZ}$; *Gjc2*$^{EGFP/EGFP}$ and *Gjb6*$^{LacZ/LacZ}$; *Gjc2*$^{+/EGFP}$ mice.

So far, functional channels formed by Cx47 and Cx30 have not been observed in vivo. Accordingly, our results suggest that in the thalamus astrocyte-to-oligodendrocyte coupling is mediated predominantly by heterotypic Cx30:Cx32 channels, while Cx43:Cx47 channels play a minor role.

Glial Cells in the Thalamus Express Unusual Antigen Profiles

As quantification indicated overlap of GS and Olig2 immunoreactivity in the thalamic networks (Fig. 5), we addressed the question of antigen profiles employing reporter mice. Slices from Cx43$^{ECFP/+}$ mice were stained against Olig2. About half of the Cx43-ECFP$^+$ cells in the thalamus coexpressed Olig2 (20 267 ± 2917 cells/mm^3 from a total of 38 563 ± 1723 ECFP$^+$ cells/mm^3) (Fig. 8*A*), while hippocampal ECFP$^+$ cells typically lacked Olig2 (3155 ± 1107 ECFP$^+$/Olig2$^+$ cells/mm^3 from a total of 52 217 ± 3215 ECFP$^+$ cells/mm^3) (Fig. 8*B*). In the neocortex 20% of the ECFP$^+$ cells expressed Olig2 (3240 ± 879 ECFP$^+$/Olig2$^+$ cells/mm^3 from a total of 15 305 ± 1126 ECFP$^+$ cells/mm^3). These data indicate the existence of an "intermediate" glial cell type in the thalamus and cortex that coexpressed astrocytic (*Gja1*) and oligodendrocytic (*Olig2*) genes. These cells proved to be mature astrocytes integrated in biocytin-labeled networks because coimmunostainig after biocytin injection revealed that in the thalamus 14% of the total number of coupled cells coexpressed of ECFP and Olig2 (58 ± 6 coupled cells, $n = 10$ slices, Supplementary Fig. 2). Brain slices from PLP-GFP mice were stained against NG2 (Trotter et al. 2010), which revealed coexpression of NG2 and GFP in the hippocampus (17.9% from a total of 26 447 ± 1434 GFP$^+$ cells/mm^3, $n = 9$ slices from 3 mice) while PLP-GFP$^+$ cells in the thalamus were not NG2$^+$ (0.2% from 158 844 ± 4092 GFP$^+$ cells/mm^3, $n = 9$ slices from 3 mice, not shown). We noted that NG2$^+$ cells were very weakly PLP-GFP$^+$. S100β is considered an astrocyte-specific marker in the hippocampus (Ogata and Kosaka 2002) and thalamus (Parri et al. 2010). In line with these previous findings, we detected only minor expression of S100β in PLP-GFP$^+$ oligodendrocytes (thalamus, 17.5%; hippocampus, 18.1%). Very few PLP-GFP$^+$ cells in the hippocampus coexpressed NG2 and S100β (1.6%) while triple labeling was not observed in the thalamus. Almost all PLP-GFP$^+$ cells in the thalamus expressed GS (94.5% from a total of 136 911 ± 9.363 GFP$^+$ cells/mm^3). In the hippocampus, GS immunoreactivity was mainly confined to astrocytes and only some GFP$^+$/GS$^+$ cells could be detected (17.8% from a total of 22 644 ± 1573 GFP$^+$ cells/mm^3; $n = 9$ slices from 3 mice, data not shown).

In another study, we used the astrocyte marker 10-formyltetrahydrofolate dehydrogenase (Aldh1L1), which revealed abundant Aldh1L1 labeling. Taking advantage of the PLP-GFP mouse line we found extensive overlap of Aldh1L1 staining and PLP-GFP in the thalamus (52% overlap from a total of 65 422 ± 6242 cells/mm^3; $n = 9$ slices from 3 mice, Supplementary Fig. 3). Almost all of these cells were also positive for the oligodendrocyte marker Olig2 (97%). Furthermore, we observed Aldh1L1 labeled cells that coexpressed Olig2 (25%). Accordingly, classical cell type markers display an overlapping expression profile in the thalamus, but barely in the hippocampus.

Discussion

Astrocytes form extensive GJNs, which are crucial for information processing (Pannasch and Rouach 2013), but such networks

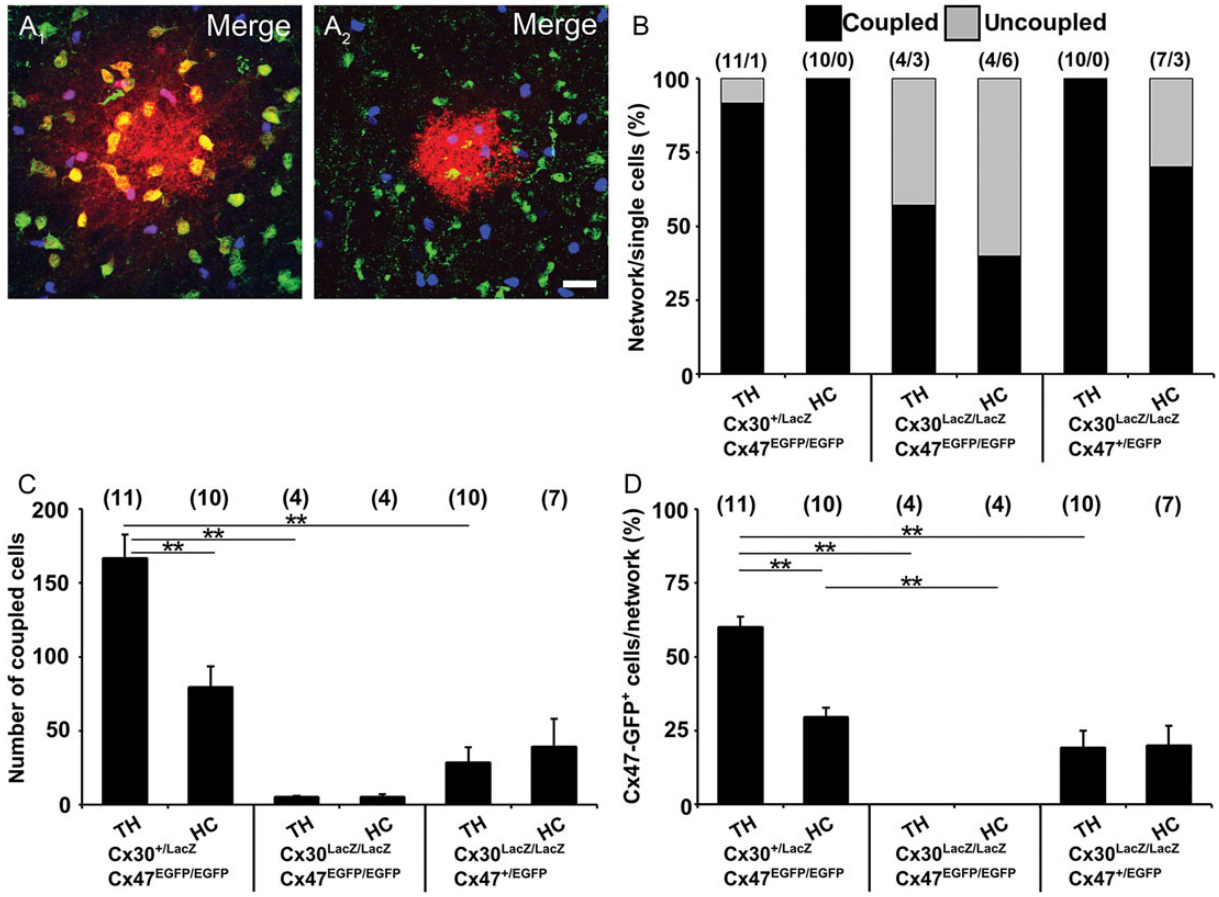

Figure 7. Panglial networks require Cx30 and Cx47 in the thalamus. Astrocytes in Cx30kiLacZ;Cx47kiEGFP mice were identified for tracer injection with SR101. Analysis of biocytin-filled networks (red) for the presence of Cx47-EGFP (green) and Cx30-LacZ (blue) expressing cells in *Gjb6*$^{+/LacZ}$;*Gjc2*$^{EGFP/EGFP}$ mice revealed panglial networks (A_1) while coupling was lacking or drastically reduced in homozygous Cx30/Cx47 (*Gjb6*$^{LacZ/LacZ}$;*Gjc2*$^{EGFP/EGFP}$) mice (A_2). Examples depict networks in the thalamus. Scale bar, 20 μm. (*B*) Three genotypes were analyzed both in hippocampus and thalamus for the proportion of coupled and uncoupled cells. (*C*) Analysis of network size revealed minimal tracer spread in Cx30/Cx47 deficient mice. (*D*) Proportion of Cx47-EGFP$^+$ oligodendrocytes. Note that oligodendrocytes were lacking in GJNs of Cx30/Cx47 deficient mice. Asterisks indicate statistical significance, number of experiments is given in parentheses.

were only analyzed in a few brain areas. Since astrocyte properties may vary across central nervous system (CNS) regions (Matyash and Kettenmann 2010; Zhang and Barres 2010), it is mandatory to extend investigation towards so far unexplored brain regions. Here, we provide the first detailed characterization of gap junction coupling in the ventrobasal thalamus and report that thalamic glial cells possess properties that are clearly distinct from those in the hippocampus or neocortex.

Our findings challenge the general assumption that Cx43 is present in all astrocytes of the brain (Nagy et al. 1997; Pannasch and Rouach 2013). First, employing Cx43kiECFP mice (Degen et al. 2012), we found that genetic deletion of one allele of Cx43 decreased coupling in the hippocampus, but not in the thalamus and cortex. Transcript and protein analyses confirmed that Cx43 is less prevalent in the thalamus. Second, 25% of SR101$^+$ astrocytes in the thalamus of Cx30 ko mice were completely uncoupled. Third, SR101 staining (Nimmerjahn et al. 2004; Kafitz et al. 2008) of acute slices from Cx43kiECFP mice revealed that many SR101$^+$ astrocytes in the thalamus lack Cx43 promoter activity. By contrast, in the hippocampus almost all SR101$^+$ astrocytes were Cx43-ECFP$^+$ (Fig. 3*B* and Degen et al. 2012). Since SR101 did not significantly colocalize with PLP-GFP, we concluded that SR101 identifies astrocytes in the thalamus. Fourth, analysis of *Gja1*$^{ECFP/+}$;*Gjb6*$^{LacZ/+}$ mice confirmed that a significant proportion of thalamic astrocytes lack Cx43. The higher proportion of Cx43-lacking astrocytes in the SR101 labeling experiment (~50%, Fig. 3*A*) compared with β-Gal/ECFP staining (20%, Fig. 4*B*) might reflect that in the latter approach ECFP detection was improved by postfixation GFP antibody staining, while in SR101 labeled slices ECFP fluorescence was directly detected. Moreover, β-Gal staining might not detect all Cx30-expressing astrocytes (Gosejacob et al. 2011). Despite these methodical limitations, our results clearly demonstrate that astrocytic coupling in the thalamus is mainly based on Cx30 and that a significant subpopulation of thalamic astrocytes lack Cx43.

A previous study, using Lucifer yellow as a tracer, found no astrocyte coupling in the ventrobasal thalamus (Parri et al. 2001). Although all glial Cxs are permeable for small molecules, permeability varies between subtypes (Elfgang et al. 1995). While the positively charged neurobiotin, which is structurally close to biocytin used here, permeates through Cx30 gap junction channels, the anionic tracer Lucifer yellow does not (Yum et al. 2007). Thus, Parri et al. (2001) indirectly confirmed the predominant role of Cx30 in thalamic gap junction coupling described in the present study.

Immunostaining revealed abundant expression of Cx26 in the thalamus (Nagy et al. 2001, 2011) although its functional

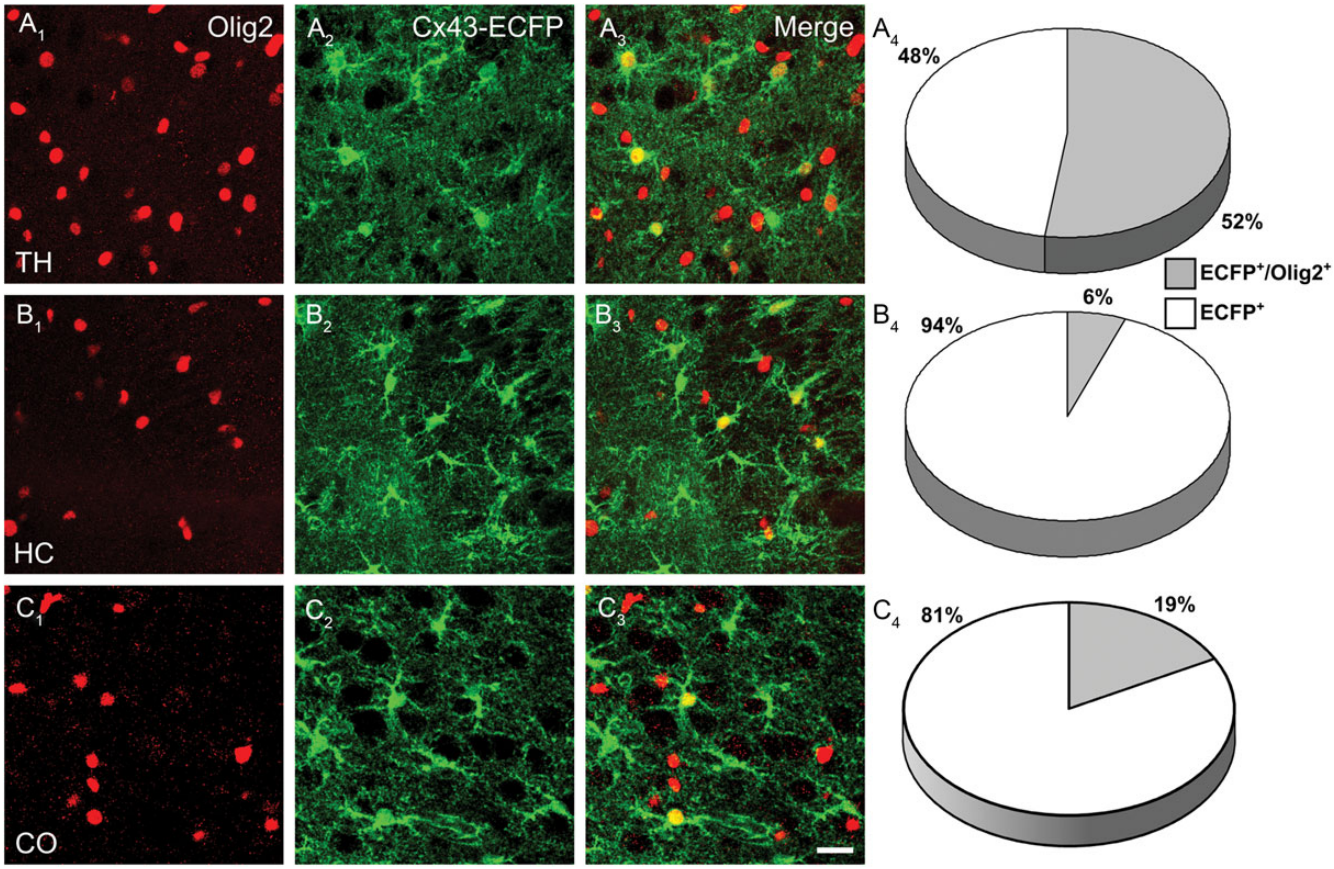

Figure 8. Thalamic Cx43-ECFP$^+$ cells express the oligodendrocyte marker Olig2. Immunostaining for Olig2 in thalamus (*A1*) and hippocampus (*B1*) was performed in heterozygous Cx43 (*Gja1*$^{ECFP/+}$) mice (*A2*, *B2*). Merged images (*A3*, *B3*) show a large overlap of ECFP and Olig2 staining in the thalamus, while in the hippocampus only very few ECFP$^+$/Olig2$^+$ cells were observed. Scale bar, 20 µm. (*A4*, *B4*) Quantitative analysis of the ECFP and Olig2 expression profile confirmed a significant difference in the antigen profile of astrocytes in both regions (overlap TH, 52.2 ± 6%; HC, 6 ± 1.8%, $n = 9$ for each region from 3 mice).

impact remained unclear yet. We addressed this question by investigating coupling in Cx26 ko mice, and our data do not indicate that this Cx significantly contributes to the GJNs. A similar conclusion can be drawn from analyses of astrocytes in mice devoid of Cx43 and Cx30, which produces uncoupling in the thalamus (this study) and hippocampus (Wallraff et al. 2006). The residual coupling we have observed in 2 astrocytes lacking Cx30 and Cx43 might reflect inefficient Cre recombination (Requardt et al. 2009). Whether Cx26 forms hemichannels or intracellular gap junctions still needs to be investigated.

So far, panglial coupling between astrocytes and oligodendrocytes *in situ* has only been detected in white matter tracts of corpus callosum and cerebellum (Maglione et al. 2010; Tress et al. 2012) while observations in neocortex were contradictory (Houades et al. 2008; Wasseff and Scherer 2011). We report abundant coupling between astrocytes and oligodendrocytes in the thalamus, hippocampus, and neocortex. Panglial coupling was observed by immunostaining of Olig2 in biocytin-filled networks and confirmed by tracer injections into PLP-GFP$^+$ cells. Notably, utilizing PLP-GFP mice we could demonstrate that more than half of the cells in thalamic GJNs were oligodendrocytes, irrespective of whether initially an astrocyte or oligodendrocyte was filled with biocytin. In the hippocampus, the size of GJNs was also independent of whether the tracer was injected into an astrocyte or oligodendrocyte, although the contribution of the latter was <15% due to the low number of PLP-GFP$^+$ cells in that region. Coupling was always bidirectional, as the extent of coupling and relative contribution of cell types to the GJNs was similar and independent of the initially injected cell type. We often observed that upon biocytin injection into astrocytes, tracer molecules spread along myelinated fiber tracts.

Gap junctions between astrocytes and oligodendrocytes are made by heterotypic channels between Cx43 (A) and Cx47 (O), or between Cx30 (A) and Cx32 (O) (Orthmann-Murphy et al. 2007). Cx47 function is directly dependent on Cx43 as the former decreases after conditional ko of Cx43 (May et al. 2013). Mutations in the Cx47 gene lead to reduced expression of myelin basic protein, astrogliosis and activation of microglia in mice (Tress et al. 2011) and Pelizaeus–Merzbacher-like disease in man (Uhlenberg et al. 2004). Genetic ablation of *Gjb6* and *Gjc2* in mice results in early onset of myelin pathology accompanied by severe motor impairments and partial premature death. In these mice complete loss of panglial networks in white matter tracts of cerebellum and corpus callosum was observed, while total network size was maintained indicating that O:O coupling was preserved (Tress et al. 2012). Whereas in the latter study oligodendrocytes were filled with the tracer, we were interested in astrocyte coupling. We observed that the thalamus of Cx30/Cx47 deficient mice was not only devoid of A:O coupling, but also almost completely lost interastrocytic coupling. This was unexpected, as Cx43-mediated

A:A coupling should have been preserved under these conditions. Interestingly, one allele of *Gjc2* was sufficient to partially restore GJNs, including panglial coupling. Thus, Cx43 expression might not only stabilize Cx47 at the oligodendrocytic surface (May et al. 2013), but in turn affects Cx43 localization. Indeed, it has been demonstrated that ko of Cx47 leads to redistribution of astrocytic Cx43 away from the oligodendrocyte plasma membrane (Li et al. 2008). Alternatively, taking into account the relatively low incidence of Cx43 in that brain region, our data might indicate that thalamic astrocytes do not form homotypic Cx43 channels. Panglial coupling in the neocortex is also mediated by Cx47, while in white matter it is still under discussion whether A:O channels are formed by Cx47 or Cx32 (Maglione et al. 2010; Wasseff and Scherer 2011). In contrast to the corpus callosum (Maglione et al. 2010), NG2 cells in the hippocampus, thalamus, and neocortex were not part of the networks.

Since GFAP is rarely expressed in thalamic astrocytes (Frassoni et al. 2000) we considered GS and Aldh1L1 as a putative astrocytic marker. As expected from the literature (Norenberg 1979; Derouiche and Frotscher 1991), we found that hippocampal GJNs mostly comprised GS^+ cells. In clear contrast, in the thalamus only a minor fraction of coupled cells stained for GS, and many of them resembled oligodendrocytes in morphology. The hypothesis that thalamic oligodendrocytes abundantly express GS was confirmed by demonstrating that almost all PLP-GFP^+ cells expressed this enzyme. Accordingly, GS is not a reliable astrocyte marker in the thalamus (see also Cammer 1990; D'Amelio et al. 1990; Miyake and Kitamura 1992; Takasaki et al. 2010). Similarly, in the thalamus Aldh1L1 colocalized with PLP and Olig2, which confirms the existence of an intermediate glial phenotype.

Based on the assumption that Cx43 expression in the brain is confined to astrocytes, we have recently generated a Cx43kiECFP mouse line and shown that in the hippocampus $ECFP^+$ cells express GFAP but not markers for neurons, NG2 cells or microglia (Degen et al. 2012). Unexpectedly, here we found that Cx43-$ECFP^+$ cells in the adult thalamus and neocortex frequently express the basic helix-loop-helix transcription factor Olig2, which is considered a marker of oligodendrocytes (Trotter et al. 2010). Existence of such an intermediate glial cell type was also in line with our coupling analysis because upon biocytin injection into astrocytes, the proportion of $Olig2^+$ cells in the networks (Fig. 5*C*) exceeded the fraction of PLP-GFP^+ oligodendrocytes (Fig. 6E_2) by ~10%. Furthermore we observed $ECFP^+$ and $Olig2^+$ cells in biocytin-labeled networks. During cortical development, Olig2 is transiently expressed in astrocytes at embryonic stages and downregulated later on. Ablation of Olig2 in astrocytes leads to a reduction in the number of astrocytes in white matter of cortex and spinal cord and to unusual, sustained expression of GFAP in cortical gray matter astrocytes (Cai et al. 2007). Fate mapping of $Olig2^+$ cells in the diencephalon revealed pronounced gliogenesis of both oligodendrocytes and astrocytes in the ventral thalamus (Ono et al. 2008). Collectively, our data suggest that in addition to *bona fide* astrocytes and oligodendrocytes, a subpopulation of glial cells in the adult thalamus have a unique, intermediate phenotype, which emphasizes the heterogeneous nature of these cells.

Tight and intimate contact and signal interaction of myelinating cells, their precursors and their enwrapped axons is necessary for the integrity of axons both in the CNS and peripheral nervous system (Nave 2010). Oligodendrocytes support axon function by transport of metabolites (Funfschilling et al. 2012; Lee et al. 2012). Because astrocytes also supply neurons with lactate in an activity-dependent manner (Pellerin and Magistretti 2012; Suzuki et al. 2011), the question arises whether lactate supply by astrocytes and oligodendrocytes is organized through parallel pathways or if panglial coupling is necessary for metabolic support of neurons and its axons. Mice lacking both oligodendrocytic Cxs, Cx32 and Cx47 show thinner and vacuolated myelin sheets and axonal degeneration (Odermatt et al. 2003; Menichella et al. 2003), which is in line with the hypothesis that panglial GJNs are crucial for nutritional supply, for example, glucose transport from blood vessels via astrocytes to oligodendrocytes and subsequent lactate transport into axons (Funfschilling et al. 2012). While previous work implied that metabolic supply of neurons only require A:A networks (Rouach et al. 2008), our data demonstrate that even in the hippocampus oligodendrocytes are part of the GJNs. Further experiments are needed to define the physiological impact of panglial coupling.

Authors' Contributions

S.G., S.P.H., G.S., M.T., H.K., and C.S. designed the research. S.G., S.P.H., G.S., and C.S. wrote the manuscript. S.G., S.P.H., P.B., J.Z., E.v.S., R.J., and N.R. conducted experiments and analyzed data. J.D., P.D., V.C., D.C., and K.W. provided new methods/reagents or tools.

Supplementary Material

Supplementary material can be found at: http://www.cercor.oxfordjournals.org/.

Funding

This work was supported by grants from the German Research Foundation (Wi 270/29-1 and 31-1, SFB 645, B2 to K.W., SFB/TR3, C1, and STE 552/4 to C.S., SFB/TR3, N01, and C9 to M.T. and K.E., 329/28 to H.K.); the Wellcome Trust (71436 to V.C.); the European Community (FP7-202167 NeuroGlia to C.S., M.T., and V.C.). D.W.C. was a Fellow of Epilepsy Research UK (P0802).

Notes

We thank Ina Fiedler, Anja Matijevic, Lukas Kunz, and Sebastian Ebert for excellent technical assistance and Dennis May for providing transgenic animals. *Conflict of Interest*: Authors declare no competing financial interests.

References

Bokor H, Acsady L, Deschenes M. 2008. Vibrissal responses of thalamic cells that project to the septal columns of the barrel cortex and to the second somatosensory area. J Neurosci. 28:5169–5177.

Bourassa J, Pinault D, Deschenes M. 1995. Corticothalamic projections from the cortical barrel field to the somatosensory thalamus in rats: a single-fibre study using biocytin as an anterograde tracer. Eur J Neurosci. 7:19–30.

Cai J, Chen Y, Cai WH, Hurlock EC, Wu H, Kernie SG, Parada LF, Lu QR. 2007. A crucial role for Olig2 in white matter astrocyte development. Development. 134:1887–1899.

Cammer W. 1990. Glutamine synthetase in the central nervous system is not confined to astrocytes. J Neuroimmunol. 26:173–178.

Coulter DA, Eid T. 2012. Astrocytic regulation of glutamate homeostasis in epilepsy. Glia. 60:1215–1226.

Crunelli V, Hughes SW. 2010. The slow (<1 Hz) rhythm of non-REM sleep: a dialogue between three cardinal oscillators. Nat Neurosci. 13:9–17.

D'Amelio F, Eng LF, Gibbs MA. 1990. Glutamine synthetase immunoreactivity is present in oligodendroglia of various regions of the central nervous system. Glia. 3:335–341.

Degen J, Dublin P, Zhang J, Dobrowolski R, Jokwitz M, Karram K, Trotter J, Jabs R, Willecke K, Steinhäuser C et al. 2012. Dual reporter approaches for identification of Cre efficacy and astrocyte heterogeneity. FASEB J. 26:4576–4583.

Dermietzel R, Traub O, Hwang TK, Beyer E, Bennett MVL, Spray DC, Willecke K. 1989. Differential expression of the three gap junction proteins in developing and mature brain tissues. Proc Natl Acad Sci USA. 86:10148–10152.

Derouiche A, Frotscher M. 1991. Astroglial processes around identified glutamatergic synapses contain glutamine synthetase: evidence for transmitter degradation. Brain Res. 552:346–350.

Elfgang C, Eckert R, Lichtenberg-Frate H, Butterweck A, Traub O, Klein RA, Hulser DF, Willecke K. 1995. Specific permeability and selective formation of gap junction channels in connexin-transfected HeLa cells. J Cell Biol. 129:805–817.

Frassoni C, Amadeo A, Ortino B, Jaranowska A, Spreafico R. 2000. Organization of radial and non-radial glia in the developing rat thalamus. J Comp Neurol. 428:527–542.

Funfschilling U, Supplie LM, Mahad D, Boretius S, Saab AS, Edgar J, Brinkmann BG, Kassmann CM, Tzvetanova ID, Mobius W et al. 2012. Glycolytic oligodendrocytes maintain myelin and long-term axonal integrity. Nature. 485:517–521.

Fuss B, Mallon B, Phan T, Ohlemeyer C, Kirchhoff F, Nishiyama A, Macklin WB. 2000. Purification and analysis of in vivo-differentiated oligodendrocytes expressing the green fluorescent protein. Dev Biol. 218:259–274.

Giaume C, Koulakoff A, Roux L, Holcman D, Rouach N. 2010. Astroglial networks: a step further in neuroglial and gliovascular interactions. Nat Rev Neurosci. 11:87–99.

Gosejacob D, Dublin P, Bedner P, Hüttmann K, Zhang J, Tress O, Willecke K, Pfrieger F, Steinhäuser C, Theis M. 2011. Role of astroglial connexin30 in hippocampal gap junction coupling. Glia. 59:511–519.

Houades V, Koulakoff A, Ezan P, Seif I, Giaume C. 2008. Gap junction-mediated astrocytic networks in the mouse barrel cortex. J Neurosci. 28:5207–5217.

Kafitz KW, Meier SD, Stephan J, Rose CR. 2008. Developmental profile and properties of sulforhodamine 101-Labelled glial cells in acute brain slices of rat hippocampus. J Neurosci Methods. 169:84–92.

Kunzelmann P, Schröder W, Traub O, Steinhäuser C, Dermietzel R, Willecke K. 1999. Late onset and increasing expression of the gap junction protein connexin30 in adult murine brain and long-term cultured astrocytes. Glia. 25:111–119.

Lee Y, Morrison BM, Li Y, Lengacher S, Farah MH, Hoffman PN, Liu Y, Tsingalia A, Jin L, Zhang PW et al. 2012. Oligodendroglia metabolically support axons and contribute to neurodegeneration. Nature. 487:443–448.

Li X, Penes M, Odermatt B, Willecke K, Nagy JI. 2008. Ablation of Cx47 in transgenic mice leads to the loss of MUPP1, ZONAB and multiple connexins at oligodendrocyte-astrocyte gap junctions. Eur J Neurosci. 28:1503–1517.

Maglione M, Tress O, Haas B, Karram K, Trotter J, Willecke K, Kettenmann H. 2010. Oligodendrocytes in mouse corpus callosum are coupled via gap junction channels formed by connexin47 and connexin32. Glia. 58:1104–1117.

Magnotti LM, Goodenough DA, Paul DL. 2011. Functional heterotypic interactions between astrocyte and oligodendrocyte connexins. Glia. 59:26–34.

Marshall CA, Novitch BG, Goldman JE. 2005. Olig2 directs astrocyte and oligodendrocyte formation in postnatal subventricular zone cells. J Neurosci. 25:7289–7298.

Matthias K, Kirchhoff F, Seifert G, Hüttmann K, Matyash M, Kettenmann H, Steinhäuser C. 2003. Segregated expression of AMPA-type glutamate receptors and glutamate transporters defines distinct astrocyte populations in the mouse hippocampus. J Neurosci. 23:1750–1758.

Matyash V, Kettenmann H. 2010. Heterogeneity in astrocyte morphology and physiology. Brain Res Rev. 63:2–10.

May D, Tress O, Seifert G, Willecke K. 2013. Connexin47 protein phosphorylation and stability in oligodendrocytes depend on expression of Connexin43 protein in astrocytes. J Neurosci. 33:7985–7996.

Menichella DM, Goodenough DA, Sirkowski E, Scherer SS, Paul DL. 2003. Connexins are critical for normal myelination in the CNS. J Neurosci. 23:5963–5973.

Miyake T, Kitamura T. 1992. Glutamine synthetase immunoreactivity in two types of mouse brain glial cells. Brain Res. 586:53–60.

Nagy JI, Li X, Rempel J, Stelmack G, Patel D, Staines WA, Yasumura T, Rash JE. 2001. Connexin26 in adult rodent central nervous system: demonstration at astrocytic gap junctions and colocalization with connexin30 and connexin43. J Comp Neurol. 441:302–323.

Nagy JI, Lynn BD, Tress O, Willecke K, Rash JE. 2011. Connexin26 expression in brain parenchymal cells demonstrated by targeted connexin ablation in transgenic mice. Eur J Neurosci. 34:263–271.

Nagy JI, Ochalski PAY, Li J, Hertzberg EL. 1997. Evidence for the co-localization of another connexin with connexin-43 at astrocytic gap junctions in rat brain. Neuroscience. 78:533–548.

Nagy JI, Rash JE. 2000. Connexins and gap junctions of astrocytes and oligodendrocytes in the CNS. Brain Res Rev. 32:29–44.

Nave KA. 2010. Myelination and support of axonal integrity by glia. Nature. 468:244–252.

Nimmerjahn A, Kirchhoff F, Kerr JN, Helmchen F. 2004. Sulforhodamine 101 as a specific marker of astroglia in the neocortex in vivo. Nat Methods. 1:31–37.

Nishiyama A, Komitova M, Suzuki R, Zhu X. 2009. Polydendrocytes (NG2 cells): multifunctional cells with lineage plasticity. Nat Rev Neurosci. 10:9–22.

Nolte C, Matyash M, Pivneva T, Schipke CG, Ohlemeyer C, Hanisch UK, Kirchhoff F, Kettenmann H. 2001. GFAP promoter-controlled EGFP-expressing transgenic mice: a tool to visualize astrocytes and astrogliosis in living brain tissue. Glia. 33:72–86.

Norenberg MD. 1979. Distribution of glutamine synthetase in the rat central nervous system. J Histochem Cytochem. 27:756–762.

Nualart-Marti A, Solsona C, Fields RD. 2013. Gap junction communication in myelinating glia. Biochim Biophys Acta. 1828:69–78.

Odermatt B, Wellershaus K, Wallraff A, Seifert G, Degen J, Euwens C, Fuss B, Bussow H, Schilling K, Steinhäuser C et al. 2003. Connexin 47 (cx47)-deficient mice with enhanced green fluorescent protein reporter gene reveal predominant oligodendrocytic expression of cx47 and display vacuolized myelin in the CNS. J Neurosci. 23:4549–4559.

Ogata K, Kosaka T. 2002. Structural and quantitative analysis of astrocytes in the mouse hippocampus. Neuroscience. 113:221–233.

Ono K, Takebayashi H, Ikeda K, Furusho M, Nishizawa T, Watanabe K, Ikenaka K. 2008. Regional- and temporal-dependent changes in the differentiation of Olig2 progenitors in the forebrain, and the impact on astrocyte development in the dorsal pallium. Dev Biol. 320:456–468.

Orthmann-Murphy JL, Freidin M, Fischer E, Scherer SS, Abrams CK. 2007. Two distinct heterotypic channels mediate gap junction coupling between astrocyte and oligodendrocyte connexins. J Neurosci. 27:13949–13957.

Pannasch U, Rouach N. 2013. Emerging role for astroglial networks in information processing: from synapse to behavior. Trends Neurosci. 36:405–417.

Pannasch U, Vargova L, Reingruber J, Ezan P, Holcman D, Giaume C, Sykova E, Rouach N. 2011. Astroglial networks scale synaptic activity and plasticity. Proc Natl Acad Sci U S A. 108:8467–8472.

Parri HR, Crunelli V. 2002. Astrocytes, spontaneity, and the developing thalamus. J Physiol Paris. 96:221–230.

Parri HR, Gould TM, Crunelli V. 2010. Sensory and cortical activation of distinct glial cell subtypes in the somatosensory thalamus of young rats. Eur J Neurosci. 32:29–40.

Parri HR, Gould TM, Crunelli V. 2001. Spontaneous astrocytic Ca2+ oscillations in situ drive NMDAR-mediated neuronal excitation. Nat Neurosci. 4:803–812.

Pellerin L, Magistretti PJ. 2012. Sweet sixteen for ANLS. J Cereb Blood Flow Metab. 32:1152–1166.

Pirttimaki TM, Hall SD, Parri HR. 2011. Sustained neuronal activity generated by glial plasticity. J Neurosci. 31:7637–7647.
Pirttimaki TM, Parri HR, Crunelli V. 2013. Astrocytic GAT-1 dysfunction in experimental absence seizures. J Physiol. 591:823–833.
Requardt RP, Kaczmarczyk L, Dublin P, Wallraff-Beck A, Mikeska T, Degen J, Waha A, Steinhäuser C, Willecke K, Theis M. 2009. Quality control of astrocyte-directed Cre transgenic mice: the benefits of a direct link between loss of gene expression and reporter activation. Glia. 57:680–692.
Rouach N, Koulakoff A, Abudara V, Willecke K, Giaume C. 2008. Astroglial metabolic networks sustain hippocampal synaptic transmission. Science. 322:1551–1555.
Roux L, Benchenane K, Rothstein JD, Bonvento G, Giaume C. 2011. Plasticity of astroglial networks in olfactory glomeruli. Proc Natl Acad Sci USA. 108:18442–18446.
Schools GP, Zhou M, Kimelberg HK. 2006. Development of gap junctions in hippocampal astrocytes: evidence that whole cell electrophysiological phenotype is an intrinsic property of the individual cell. J Neurophysiol. 96:1383–1392.
Seifert G, Hüttmann K, Binder DK, Hartmann C, Wyczynski A, Neusch C, Steinhäuser C. 2009. Analysis of astroglial K+ channel expression in the developing hippocampus reveals a predominant role of the Kir4.1 subunit. J Neurosci. 9:7474–7488.
Sonnewald U, Westergaard N, Schousboe A. 1997. Glutamate transport and metabolism in astrocytes. Glia. 21:56–63.
Steriade M. 2006. Grouping of brain rhythms in corticothalamic systems. Neuroscience. 137:1087–1106.
Suzuki A, Stern SA, Bozdagi O, Huntley GW, Walker RH, Magistretti PJ, Alberini CM. 2011. Astrocyte-neuron lactate transport is required for long-term memory formation. Cell. 144:810–823.
Takasaki C, Yamasaki M, Uchigashima M, Konno K, Yanagawa Y, Watanabe M. 2010. Cytochemical and cytological properties of perineuronal oligodendrocytes in the mouse cortex. Eur J Neurosci. 32:1326–1336.
Teubner B, Michel V, Pesch J, Lautermann J, Cohen-Salmon M, Sohl G, Jahnke K, Winterhager E, Herberhold C, Hardelin JP et al. 2003. Connexin30 (Gjb6)-deficiency causes severe hearing impairment and lack of endocochlear potential. Hum Mol Genet. 12:13–21.
Theis M, Giaume C. 2012. Connexin-based intercellular communication and astrocyte heterogeneity. Brain Res. 1487:88–98.
Tress O, Maglione M, May D, Pivneva T, Richter N, Seyfarth J, Binder S, Zlomuzica A, Seifert G, Theis M et al. 2012. Panglial gap junctional communication is essential for maintenance of myelin in the CNS. J Neurosci. 32:7499–7518.
Tress O, Maglione M, Zlomuzica A, May D, Dicke N, Degen J, Dere E, Kettenmann H, Hartmann D, Willecke K. 2011. Pathologic and phenotypic alterations in a mouse expressing a connexin47 missense mutation that causes Pelizaeus–Merzbacher-like disease in humans. PLoS Genet. 7:e1002146.
Trotter J, Karram K, Nishiyama A. 2010. NG2 cells: properties, progeny and origin. Brain Res Rev. 63:72–82.
Uhlenberg B, Schuelke M, Ruschendorf F, Ruf N, Kaindl AM, Henneke M, Thiele H, Stoltenburg-Didinger G, Aksu F, Topaloglu H et al. 2004. Mutations in the gene encoding gap junction protein alpha 12 (connexin 46.6) cause Pelizaeus–Merzbacher-like disease. Am J Hum Genet. 75:251–260.
Wallraff A, Kohling R, Heinemann U, Theis M, Willecke K, Steinhäuser C. 2006. The impact of astrocytic gap junctional coupling on potassium buffering in the hippocampus. J Neurosci. 26:5438–5447.
Wasseff SK, Scherer SS. 2011. Cx32 and Cx47 mediate oligodendrocyte:astrocyte and oligodendrocyte:oligodendrocyte gap junction coupling. Neurobiol Dis. 42:506–513.
Yum SW, Zhang J, Valiunas V, Kanaporis G, Brink PR, White TW, Scherer SS. 2007. Human connexin26 and connexin30 form functional heteromeric and heterotypic channels. Am J Physiol Cell Physiol. 293:C1032–C1048.
Zhang Y, Barres BA. 2010. Astrocyte heterogeneity: an underappreciated topic in neurobiology. Curr Opin Neurobiol. 20:588–594.